Determination of molecular contributions to the nonlinear refractive index of air for mid-infrared femtosecond laser-pulse excitation

D. Langevin,[1] J. M. Brown,[1,2] M. B. Gaarde,[2] and A. Couairon[1]

[1]*Centre de Physique Théorique, Ecole Polytechnique, CNRS, F-91128 Palaiseau, France*
[2]*Department of Physics and Astronomy, Louisiana State University, Baton Rouge, Louisiana 70803-4001, USA*

Numerical simulations of the rotational contribution of oxygen and nitrogen molecules to the Kerr refractive index change in air are performed for ultrashort laser pulses in the near- and mid-infrared wavelength region. The calculated molecular response is parametrized by means of a damped harmonic oscillator model that is easily tractable in numerical simulations of long-distance propagation of ultrashort laser pulses. Our simulations show that pulses from available mid-infrared laser systems are long enough to be dramatically affected by the molecular response of air during propagation.

I. INTRODUCTION

Laser filamentation in air is a nonlinear optical phenomenon where a laser pulse propagates over an extended distance, with a near constant beam diameter and a high intensity core that is sustained by competing linear and nonlinear effects. The most important effects are linear diffraction and dispersion, which spread the frequency components in space and time, respectively, nonlinear self-focusing due to the third-order polarization, and ionization contributions [1]. The applications using precise control of filaments are numerous, and include atmospheric measurements [2,3], channeling of high power beams [4], and lightning protection [2,5]. With the recent development of high-power mid-infrared (MIR) laser sources [6,7], there is tremendous interest in harnessing filamentation in this wavelength regime, where many applications in strong-field physics could benefit greatly from the favorable wavelength scaling [8]. Many of the nonlinear optical parameters used in modeling the propagation of MIR laser pulses are relatively unknown in this newly accessible region of the spectrum. Recent studies have indicated that ionization may play a smaller role than at near-infrared (NIR) wavelengths, and that low-order harmonics and their propagation over a large spectral bandwidth may be more important in controlling the spatial-temporal dynamics [9,10].

Beam self-focusing is the most important effect for opposing the effect of diffraction and producing a filament. This nonlinear effect is modeled as an intensity dependent change in the refractive index using a nonlinear refractive index coefficient n_2. The total index of refraction of the medium is then $n = n_0 + n_2 I$, where n_0 is the linear refractive index and I is the laser-pulse intensity. In a molecular gas, there are two contributions to the nonlinear refractive index. The first is the instantaneous (Kerr) contribution from the electronic response to the electric field, and is proportional to the third-order susceptibility. The second is time dependent and arises from the tendency of molecules to align themselves with the polarization of the electric field. Since the polarizability in general depends on the molecular alignment, this in turn changes the electronic response. This delayed response (Raman-Kerr), manifests itself in propagation as an increase in the refractive index near the trailing end of the pulse. This increase of index can offset a decrease arising from plasma effects and can greatly modify the dispersion landscape that is seen by the propagating laser pulse [11]. For example, it is well known that the nonlinear phase modification of the Raman-Kerr response results in a redshift of the laser spectrum [12].

In the NIR spectral region, the instantaneous and rotational responses have been successfully modeled using a nonlinear polarization,

$$P_{\text{NL}}(t, r, z) = \epsilon_0 \chi^{(3)} \Bigg[(1 - f_R) E^2(t, r, z) + f_R \int_{-\infty}^{t} R(t - t') E^2(t', r, z) dt' \Bigg] E(t, r, z),$$

$$(1)$$

where $\chi^{(3)}$ denotes the total (electronic and molecular) third-order susceptibility, and f_R denotes the Raman-Kerr (molecular) fraction. The molecular response $R(t)$ is modeled as a damped harmonic oscillator [13] and takes the form of

$$R(t) = R_0 \exp(-\Gamma t/2) \sin(\Lambda t), \qquad (2)$$

where $R_0 \equiv (\Gamma^2/4 + \Lambda^2)\Lambda^{-1}$ represents a normalization factor, and Γ and Λ are the characteristic frequencies. The use of the parametrization in Eq. (2) means that the molecular response is assumed to be *independent* of the pulse shape and intensity, which is crucial for macroscopic laser propagation calculations in which the laser field changes shape in space, time, and frequency.

In this paper, we show that this treatment can be extended to the molecular response at MIR wavelengths. We calculate the parameters needed for $R(t)$ and show that they are valid over a range of pulse durations and wavelengths. We follow the approach of Ortigoso *et al.* [14] and calculate the rotational molecular response by solving the time-dependent

Schrödinger equation (TDSE) using a basis of pendular (field-free rotational) states. We then fit the rotational response of an ensemble of molecules at thermal equilibrium to the convolution (second term) in Eq. (1), with $R(t)$ given by Eq. (2), and extract values for the characteristic frequencies Γ and Λ. Finally, we show that the rotational contribution to the nonlinear refractive index dramatically impacts the propagation of MIR pulses from sources that are currently available or will be available in the near future. Therefore, the inclusion of the rotational response in the medium modeling equations is necessary for accurate simulations of MIR laser-pulse propagation experiments in air.

II. METHODS

A. Macroscopic laser propagation model

Models for nonlinear laser-pulse propagation couple a propagation equation with a set of medium response functions that take the form of a field-dependent nonlinear polarization and a nonlinear current. When propagation is essentially unidirectional, a standard model used is the unidirectional pulse propagation equation (UPPE) written in the spectral domain for the Fourier components of the electric field $\mathcal{E}(\omega, k_\perp, z)$. In cylindrical coordinates, these components are obtained using the Fourier-Hankel transform of the electric field $\mathcal{F}[E(t, r, z)]$ [15,16],

$$\frac{\partial \mathcal{E}}{\partial z} = ik_z(\omega, k_\perp)\mathcal{E} + \frac{i}{2\epsilon_0 c n(\omega)}(\omega \mathcal{P} + i\mathcal{J}), \quad (3)$$

where $k_z(\omega, k_\perp) = \sqrt{k^2(\omega) - k_\perp^2}$. The material dispersion is taken into account by the frequency dependence of the linear refraction index $n(\omega)$, via the propagation constant $k(\omega) = n(\omega)\omega/c$. The constants ϵ_0 and c denote the vacuum permittivity and the velocity of light. The nonlinear polarization $\mathcal{P}(\omega, k_\perp, z)$ and current $\mathcal{J}(\omega, k_\perp, z)$ are obtained by Fourier-Hankel transforms of their space-time counterparts $P(t, r, z)$ and $J(t, r, z)$.

In this paper we focus on the Kerr response of air, hence, we only consider the third-order nonlinear polarization, which includes two different terms corresponding to the electronic and molecular contributions as shown in Eq. (1).

B. Microscopic model of molecular rotation

The rotational Raman contribution to the nonlinear index arises from the alignment of molecules interacting with the laser field. The molecular alignment degree can be numerically calculated using an effective Hamiltonian that acts on the vibronic ground state [14,17]. We follow this approach and present the main steps of the model in this section. To model the time evolution of the molecule, the total wave function is described by a combination of field-free rotational states $|\psi(t)\rangle = d_{J,M}(t)|JM\rangle$, where $|JM\rangle$ are the spherical harmonic functions $Y_{J,M}$. The wave function satisfies the time-dependent Schrödinger equation

$$i\hbar \frac{\partial |\psi\rangle}{\partial t} = H_e |\psi\rangle, \quad (4)$$

where

$$H_e = B\mathbf{J}^2 - \frac{E^2(t)}{2}[\Delta\alpha \cos^2\theta(t) + \alpha_\perp] \quad (5)$$

is the effective Hamiltonian, $E(t)$ denotes the electric field, and $\theta(t)$ is the angle between the molecule axis and laser polarization. The linear optical properties of the molecule are captured by the polarizability difference $\Delta\alpha \equiv \alpha_\parallel - \alpha_\perp$, where $\alpha_\parallel$ and $\alpha_\perp$ denote the parallel and perpendicular polarizabilities of the molecule.

The energy of the molecule in a specific angular momentum state is proportional to the expectation values of the operator $\mathbf{J}^2$ through the relation

$$\langle JM|B\mathbf{J}^2|JM\rangle \equiv B_0 J(J+1) - D_0 J^2(J+1)^2 = E_J, \quad (6)$$

where B_0 and D_0 are the rovibrational molecular constants [14,17,18]. The values for nitrogen and oxygen in units of cm^{-1} are

$$B_0^{N_2} = 1.9896, \quad D_0^{N_2} = 5.76 \times 10^{-6}, \quad (7)$$

$$B_0^{O_2} = 1.4219, \quad D_0^{O_2} = -4.86 \times 10^{-6}. \quad (8)$$

Inserting the total wave function $|\psi(t)\rangle$ into the TDSE gives a large system of ordinary differential equations for the time-dependent probability amplitudes $d_{J,M}(t)$,

$$i\hbar \frac{d}{dt} d_{J,M}$$
$$= d_{J,M}(t)\left(B\langle J, M| \mathbf{J}^2 |J, M\rangle - \alpha_\perp \frac{E^2(t)}{2}\right)$$
$$- \sum_{J',M'} d_{J',M'}(t)\Delta\alpha \frac{E^2(t)}{2}\langle J, M| \cos^2\theta(t)|J', M'\rangle, \quad (9)$$

where the matrix elements $\langle JM|\cos^2\theta(t)|J'M'\rangle$ only couple $J \leftrightarrow J'$ and $J \leftrightarrow J' \pm 2$ momentum values. The time evolution of the system as it interacts with the laser field is solved using a fourth-order Runga-Kutta method with adaptive step control. The observable of interest for a single molecule is the alignment degree $\langle \cos^2\theta(t)\rangle$ which is calculated from the values of $d_{J,M}(t)$ and using the 3-j Wigner symbols that describe coupling between states:

$$\langle \cos^2(\theta(t))\rangle = \sum_{J,J'} d_{J,M}(t) d_{J',M'}(t) \times (2J+1)^{1/2}(2J'+1)^{1/2}$$
$$\times \begin{pmatrix} J & 2 & J' \\ -M & 0 & M \end{pmatrix}\begin{pmatrix} J & 2 & J' \\ 0 & 0 & 0 \end{pmatrix}. \quad (10)$$

We assume that air consists of a thermalized ensemble of nitrogen and oxygen molecules, which can be ascribed a rotational temperature T_r before the arrival of the pulse. The ensemble of molecules is assumed to follow a temperature-dependent Boltzmann distribution of the initial molecular states $|J_0 M_0\rangle$, with statistical weight $\rho_J = Q_r^{-1} \exp(-E_J/k_B T_r)$, where $Q_r = \sum_J (2J+1)\exp(-E_J/k_B T_r)$ denotes the rotational partition function and $T_r = 293$ K in all calculations.

The molecular alignment degree of an ensemble of molecules is denoted by $\langle\langle \cos^2\theta(t)\rangle\rangle$ and is represented as an ensemble average of all contributions $\langle \cos^2\theta(t)\rangle_{J_0 M_0} =$
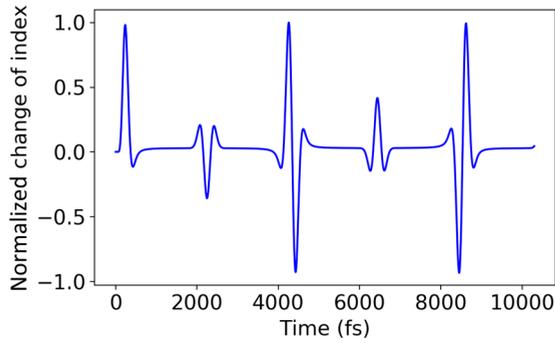
FIG. 1. Computed evolution of the rotational contribution to the nonlinear index of nitrogen [Eq. (12)], showing periodic resurgences of molecular alignment.

$\langle \psi_{J_0 M_0}(t) | \cos^2 \theta(t) | \psi_{J_0 M_0}(t) \rangle$, where $\psi_{J_0 M_0}(t)$ denotes the rotational wave packet at time t that evolved from the initial state $\psi_{J_0 M_0}(t=0) = |J_0 M_0\rangle$, by weighting the contribution of each initial molecular state by ρ_{J_0}:

$$\langle\langle \cos^2 \theta(t) \rangle\rangle = \sum_{J_0, M_0} \rho_{J_0} \langle \cos^2[\theta(t)] \rangle_{J_0, M_0}. \qquad (11)$$

The change in the index of refraction due to the average alignment of the ensemble of molecules is

$$\Delta n_{\rm rot} = \frac{N \Delta \alpha}{n_0 \epsilon_0} [\langle\langle \cos^2 \theta(t) \rangle\rangle - 1/3] \qquad (12)$$

where $N = 2.5 \times 10^{19}$ cm^{-3} is the initial molecular density, $\Delta \alpha = \alpha_\parallel - \alpha_\perp$ is the polarizability difference [17], and n_0 is the linear refractive index at the fundamental frequency ω_0.

An example of a calculation of the change in refractive index due to the rotational response, Eq. (12), for nitrogen molecules is displayed in Fig. 1. The driving field has a central wavelength of 1 μm, a peak intensity of 20 TW/cm^2, and pulse duration of 30 fs. Periodic variations to the refractive index change are visible long after the end of the pulse and these resurgences are caused by the realignment of the different rotational modes appearing every 8.4 ps. Resurgences of molecular alignment were investigated as a practical tool for controlling the properties of an intense probe pulse that undergoes filamentation in the wake of a pump pulse that aligns the molecules [19–22]. In this paper, we focus on the molecular response for short times (<1 ps) after the driving pulse.

C. Parametrization of rotational response

It would be extremely computationally demanding to calculate the molecular response, Eq. (11), for each grid point in space and time during the laser propagation simulation. This advocates for a parametrized representation of the molecular response, such as that in Eqs. (1) and (2). At 800 nm it has been demonstrated [13] that the molecular response of air after excitation by an ultrashort laser pulse can be parametrized using a damped harmonic oscillator model, taking the form of Eqs. (1) and (2). This parametrization is advantageous when the model needs to capture the change in the refractive index on a time scale similar to that of the laser-pulse duration (a few hundred femtoseconds), corresponding to the first peak in
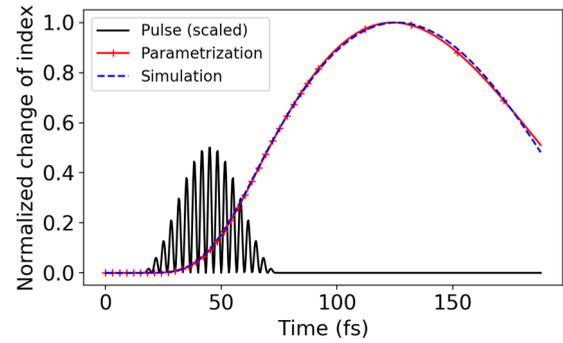
FIG. 2. Parametrization of the change of Raman-Kerr index with a damped oscillator response model for nitrogen, and a driving pulse with wavelength of 2 μm, intensity of 2×10^{12} W/cm^2, and pulse duration of 30 fs. Parameter values found by the fitting procedure are $\Gamma = 7.57$ THz and $\Lambda = 16.7$ THz.

Fig. 1. In this section, we show how the parametrization that was performed in the NIR can be extended into the MIR.

The goal of the parametrization is to be able to equate the relation between the rotational contribution to the nonlinear index in Eq. (1) and the averaged degree of molecular alignment, Eq. (12),

$$n_{2,\rm rot} \int_{-\infty}^{t} R(t - t')I(t')dt' = \frac{N \Delta \alpha}{n_0 \epsilon_0}[\langle\langle \cos^2 \theta(t) \rangle\rangle - 1/3],$$
$$(13)$$

where $I = \epsilon_0 c n_0 E^2 / 2$ denotes the intensity linked to the propagating electric field,

$$E(t) = E_0 \cos(\omega_0 t) \cos\left(\frac{\pi t}{2T}\right), \qquad (14)$$

and E_0 denotes the peak field (peak intensity I_0), T the full width at half maximum (FWHM) pulse duration. *A priori* it is not obvious that such a parametrization can be performed in the MIR and to what extent the various parameters in the model ($n_{2,\rm rot}$, Λ, Γ) are dependent on wavelength, intensity, and pulse duration.

The first step in the parametrization is to extract the frequency parameters Λ and Γ. A quantum calculation is performed to retrieve the alignment degree $\langle\langle \cos^2 \theta(t) \rangle\rangle$ of Eq. (13). Both sides of Eq. (13) are independently normalized so that their maximum value is unity. Using a nonlinear least-squares fitting procedure, we are able to find a set of characteristic frequencies, Γ and Λ, that provide good agreement between the normalized quantum and classical responses. An example of this fitting is shown in Fig. 2, where the damped harmonic oscillator agrees well with the molecular response from the quantum simulation.

This procedure for finding Γ and Λ is performed for a wide range of peak laser intensities up to 20 TW/cm^2. We observe that the Γ and Λ parameters are fairly constant, indicating that the molecular response shape is universal, and that any intensity dependence of the response can be captured by a multiplicative factor, shown in Eq. (13) as $n_{2,\rm rot}$.

The resulting maximum change in the refractive index as a function of peak laser intensity is plotted in Fig. 3.

We observe that the strength of the response is a linear function of the peak field intensity. This means that the
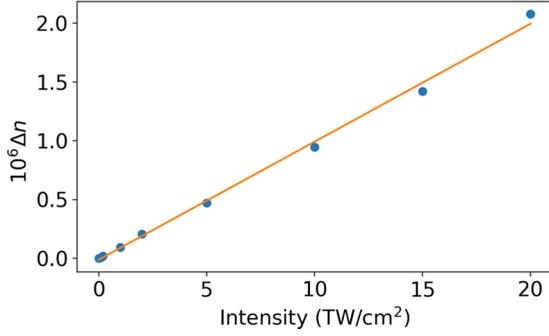
FIG. 3. Linear fit (orange line) of the maximum change of the Raman-Kerr index (blue circles) as a function of peak laser intensity I_0.

FIG. 5. Nonlinear index coefficients for N_2 and O_2 as a function of the central wavelength of the laser pulse (adapted from results in Ref. [23]).

molecular response obtained by the quantum calculation, i.e., the right-hand side in Eq. (13), is proportional to the pulse intensity I_0. Therefore, the nonlinear Raman-Kerr coefficient $n_{2,\mathrm{rot}}$ can simply be obtained as the slope of the refractive index change versus intensity after scaling the quantum response by the values for polarizability anistropy $\Delta\alpha$ and the density of neutrals N. The values used for polarizability anisotropies were calculated from data in [23] and plotted in Fig. 4.

In nonlinear optics, it is customary to work with the nonlinear index coefficient linked to the third-order susceptibility by the relation $\chi^{(3)} = (4/3)\epsilon_0 cn_2 n_0^2$. We follow this usage and define $n_2 = n_{2,\mathrm{rot}} + n_{2,\mathrm{inst}}$ as the total nonlinear index coefficient, $n_{2,\mathrm{rot}}$ as the molecular (rotational) contribution to this index, and $n_{2,\mathrm{inst}}$ as the electronic (instantaneous) contribution. The instantaneous nonlinear index coefficient $n_{2,\mathrm{inst}}$ and its dependence upon laser wavelength is known up to 4 μm from [23]. Figure 5 shows the dispersion of the nonlinear index coefficients for nitrogen and oxygen molecules. Using these values for $n_{2,\mathrm{inst}}$ we are able to determine $n_{2,\mathrm{rot}}$ for MIR pulses, and therefore the fraction of molecular (rotational, or delayed) contribution is $f_R = n_{2,\mathrm{rot}}/n_2$.

We distinguish parameters for the molecular response of N_2, O_2, and air. We determine the molecular responses for nitrogen and oxygen first, as if they were pure gases. In a second step, we consider air as a mixture with 21% of oxygen and 79% of nitrogen. The nonlinear polarization of air can simply be written as a weighed sum,

$$P^{(\mathrm{air})} = \sum_{(c)} x_{(c)} P^{(c)} = 0.21 P^{(\mathrm{O}_2)} + 0.79 P^{(\mathrm{N}_2)}, \quad (15)$$

where for each constituent $(c) = \mathrm{O}_2, \mathrm{N}_2$, with fraction $x_{(c)} = 0.21, 0.79$, the nonlinear polarization $P^{(c)}$ follows Eqs. (1) and (2), with corresponding parameters $f_R^{(c)}$, $\Gamma^{(c)}$, and $\Lambda^{(c)}$. However, we also determined a parametrization of air using a single response function in the form of (2) with parameters $f_R^{(\mathrm{air})}$, $\Gamma^{(\mathrm{air})}$, and $\Lambda^{(\mathrm{air})}$ determined from a weighed version of Eq. (13):

$$f_R^{(\mathrm{air})} n_2^{(\mathrm{air})} \int_{-\infty}^{t} R^{(\mathrm{air})}(t - t')I(t')dt'$$

$$= \frac{N}{n_0 \epsilon_0} \sum_{(c)} x_{(c)} \Delta\alpha^{(c)} [\langle\langle \cos^2\theta^{(c)}(t) \rangle\rangle - 1/3]. \quad (16)$$

III. RESULTS

We determined the parameter values Γ, Λ, $n_{2,\mathrm{rot}}$, and f_R for the molecules N_2 and O_2 over a wide range of laser-pulse durations ranging from 10 to 500 fs, wavelengths ranging from 0.8 to 4 μm, and intensities up to 20 TW/cm^2.

A. Raman-Kerr response of N_2

Figure 6(a) shows calculations of Γ and Λ for a range of different wavelengths and pulse durations. The figure demonstrates that Γ and Λ are essentially independent of wavelength, but exhibit a moderate dependence on the pulse duration. Λ only moderately decreases for increasing pulse durations with an average value of $\Lambda \sim 15$ THz. Values for Γ range from 7 to 16 THz.

Figure 6(b) shows a smooth variation of the Raman-Kerr fraction with the pulse duration, with values ranging from 0.55 to 0.7. The Raman-Kerr fraction is nearly wavelength independent in the near- and mid-infrared region but a small variation of a few percent is found in the near infrared.

The values plotted in Fig. 6 can be directly used in simulations using the model Eqs. (1)–(3). However, these values do not indicate whether we should expect a significant contribution of the Raman-Kerr effect. Indeed, the Raman-Kerr

FIG. 4. Polarizability anisotropy for N_2 and O_2 as a function of the central wavelength of the laser pulse (adapted from results in Ref. [23]). The arrows indicate the associated scale for each curve.
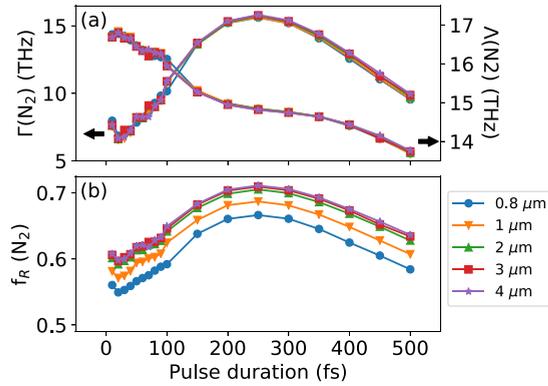
FIG. 6. Parametrization of the Raman-Kerr response for N$_2$. (a) Values of parameters Γ and Λ (arrows indicate the associated scale for each curve). (b) The Raman-Kerr fraction f_R as functions of the pulse duration for wavelengths of 0.8–4 μm.

effect is implemented as a convolution between the laser field and response function [Eq. (1)], therefore its effect is only significant when there is a large temporal overlap. A criterion for easily quantifying this overlap amounts to comparing the pulse duration and the position of the maximum of the material response. The time at which the peak of the response function occurs can be found by taking the temporal derivative of Eq. (2) and is $t_p = \Lambda^{-1} \tan^{-1}(2\Lambda/\Gamma)$. From the calculated values of Λ and Γ, t_p is found to range between 75 and 90 fs, which roughly indicates the pulse duration above which the Raman-Kerr effect will have a significant contribution to the refraction index change. The Raman-Kerr contribution of nitrogen molecules can be neglected for pulses of significantly shorter duration than 75 fs. This is consistent with measurements performed at a laser wavelength of 0.8 μm [11,24,25].

B. Raman-Kerr response of O$_2$

The parametrization of the molecular response of O$_2$ is presented in Fig. 7 for the same parameter range as for nitrogen. The two frequencies parametrizing the oxygen response, Γ and Λ, have the same behavior and order of magnitude
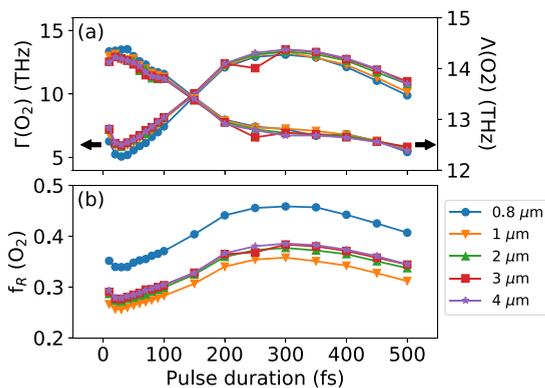
FIG. 7. Parametrization of the Raman-Kerr response for O$_2$. (a) Values of parameters Γ and Λ (arrows indicate the associated scale for each curve). (b) The Raman-Kerr fraction f_R as functions of the pulse duration for wavelengths of 0.8–4 μm.
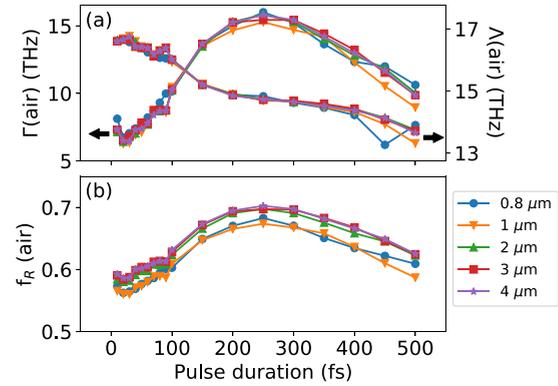
FIG. 8. Parametrization of the Raman-Kerr response for air. (a) Values of parameters Γ and Λ (arrows indicate the associated scale for each curve). (b) The Raman-Kerr fraction f_R as functions of the pulse duration for wavelengths of 0.8–4 μm.

as the corresponding parameters for nitrogen. The values for Γ and Λ are slightly lower for oxygen than for nitrogen. In contrast, the values for the fraction of the Raman-Kerr index is significantly lower for oxygen, ranging from 25 to 45%. At first glance it may be surprising that the larger polarization anistropy $\Delta\alpha$ for O$_2$ does not lead to a larger overall contribution of the delayed response (larger f_R) compared to N$_2$. This indicates that the convolution integral in Eq. (1) plays a
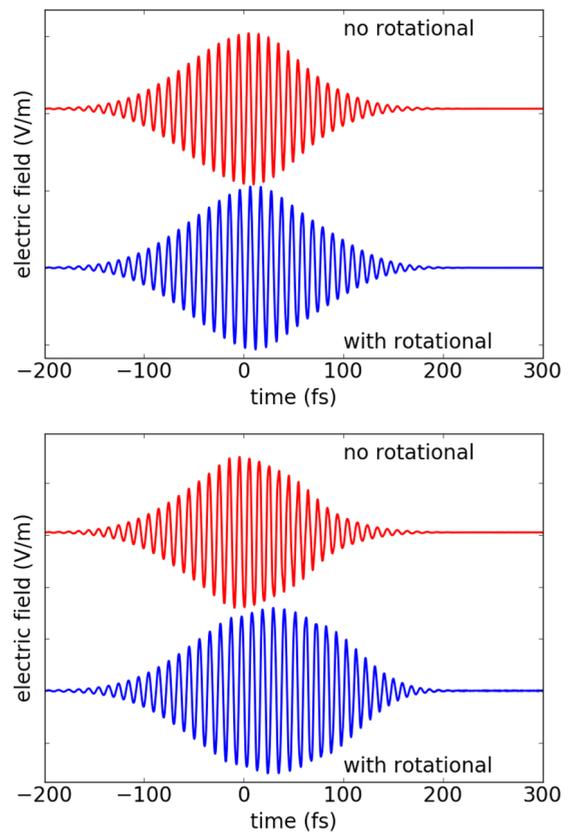
FIG. 9. The on-axis electric field after 200 cm of propagation for the cases of with and without the delayed Raman-Kerr response. Top: 20 mJ; bottom: 40 mJ.
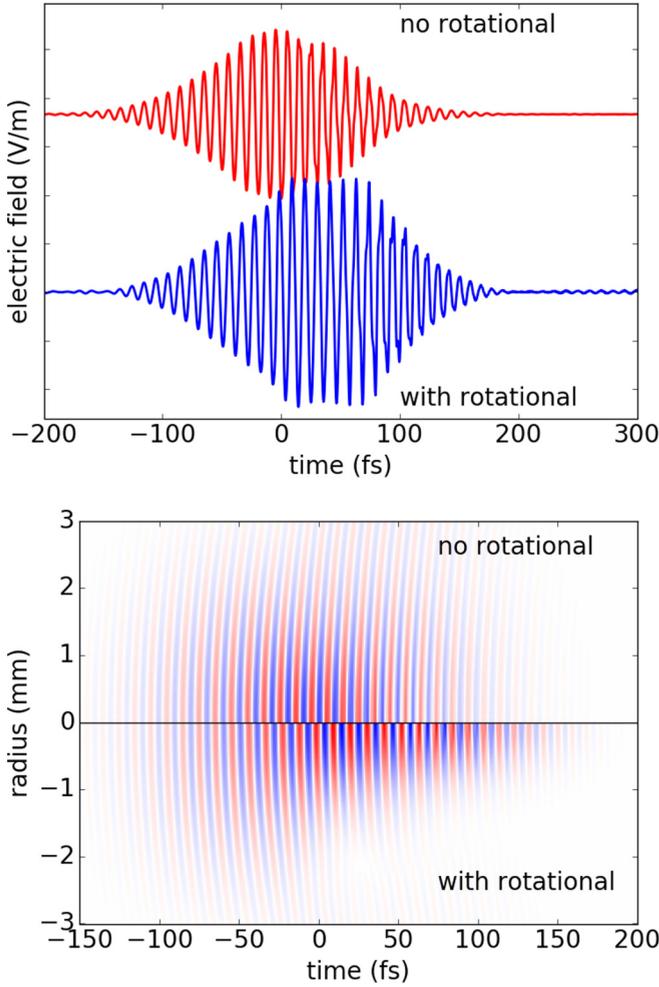
FIG. 10. The on-axis (top) and spatial-temporal (bottom) profile of the electric field for the 60-mJ pulse after 200 cm of propagation.

significant role in determining the relative strengths between the instantaneous and delayed responses. Given that the fitted values of Γ and Λ are different between the two species leads to a large difference in f_R. The lower molecular contribution of oxygen in conjunction with the 21/79 ratio of oxygen molecules in air indicates that the molecular contribution to the nonlinear index in air is essentially due to nitrogen molecules.

C. Raman-Kerr response of air

To parametrize the Raman-Kerr response of air, we used the procedure described by Eq. (16). The results are presented in Fig. 8, for wavelengths ranging from 0.8 to 4 μm and pulse durations ranging from 10 to 500 fs. The two characteristic frequencies again have similar behavior and order of magnitude as the corresponding quantities for nitrogen and oxygen, i.e., $6 \leqslant \Gamma \leqslant 16$ THz and $13 \leqslant \Lambda \leqslant 17$ THz. The Raman-Kerr fraction for air lies above 0.6 for these pulse durations, indicating that the molecular contribution to the Kerr effect is slightly stronger than the electronic contribution for most currently available ultrashort laser sources from the near- to the mid-infrared wavelength region. We note that the
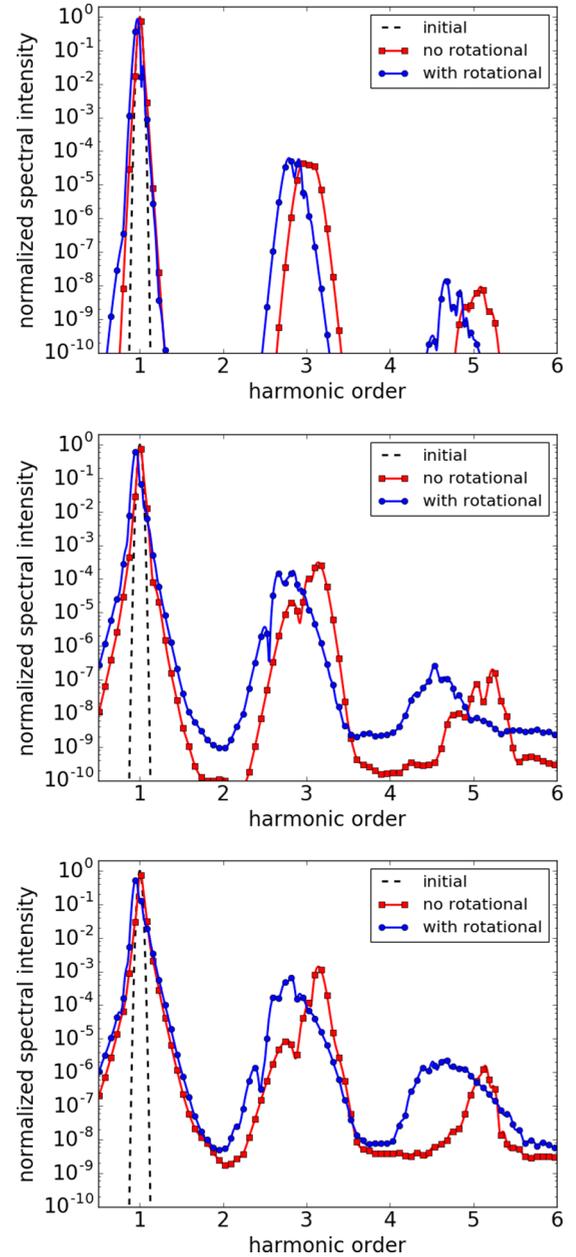
FIG. 11. The initial and far-field spectra of a 100-fs laser pulse after 200 cm of propagation for the cases with and without the delayed Raman-Kerr response. Top: 20 mJ; middle: 40 mJ; bottom: 60 mJ.

values found at 800 nm are in good agreement with the earlier determination of 0.5 for this coefficient [24].

Finally, we emphasize that the values for the two frequencies, Γ and Λ, produce a response function whose peak is around $t_p \sim 75$ fs. Therefore, we conclude that the Raman-Kerr effect is significant for laser-pulse durations of ~ 75 fs and longer.

IV. RAMAN-KERR EFFECT IN LASER PROPAGATION

We demonstrate the effect of including the Raman-Kerr contribution in laser propagation simulations by focusing a MIR laser pulse in air using a parabolic mirror with a focus of 100 cm. The laser has a wavelength of 3 μm, a $1/e^2$ radius of

1 mm, and a full width at half maximum duration of 100 fs. We varied the pulse energies from 20 to 60 mJ, where 60 mJ corresponds to 3.1 times the critical power. To model the nonlinear properties of air we used the value of instantaneous nonlinear index $n_{2,\text{inst}} = 7.8 \times 10^{20}$ cm^2/W and the extracted value of the rotational index $n_{2,\text{rot}} = 14 \times 10^{20}$ cm^2/W from the parametrization.

In Fig. 9, the on-axis electric fields are plotted for pulse energies of 20 and 40 mJ pulses after 200 cm of propagation for both cases of with and without the Raman-Kerr effect. Filamentation starts after the nonlinear focus, the position of which is shifted to longer distances when the Raman-Kerr effect is playing a role, in keeping with a scaling law proposed in Ref. [26] that extends Marburger's law [27]. The effect of including the Raman-Kerr effect is visible at the trailing end of the pulse as a phase change of the electric field and an increase in its magnitude. The effect is even more dramatic at a pulse energy of 60 mJ (displayed in Fig. 10). The increase in the field magnitude is due to a focusing effect that arises from an increase in refractive index as the molecules begin to align with the laser polarization. The Raman-Kerr effect also significantly modifies the spectrum of the laser pulse. Since the trailing part of the pulse experiences a temporally increasing index of refraction, the carrier field is elongated, resulting in an asymmetric redshift of the pulse spectrum. The far-field spectra for laser-pulse energies of 20, 40, and 60 mJ are plotted in Fig. 11. From the top plot of Fig. 11 the redshift of the fundamental is estimated to be between 0.05 and 0.1 harmonic order. Since the third harmonic is generated through a $\chi^{(3)}$ process involving three photons of the fundamental (third-harmonic generation $\omega + \omega + \omega \to 3\omega$), it is redshifted approximately three times more than the fundamental resulting in a shift of around 0.2–0.3 harmonic order.

As the laser energy increases to 40–60 mJ, the spectral broadening of the fundamental becomes more significant due to self-phase modulations. For third-harmonic generation, this results in a wider spectrum around the redshifted third harmonic. For fifth-harmonic generation, among the different competing processes, four-wave mixing ($\omega + \omega + 3\omega \to 5\omega$) prevails. It involves two fundamental photons and one third-harmonic photon from already broadband and redshifted spectra, resulting in even larger shifts of the fifth harmonic.

V. CONCLUSION

In conclusion, we investigated the molecular contributions to the nonlinear refractive index of air for mid-infrared femtosecond laser-pulse excitation. From quantum numerical simulations, we obtained the molecular response on nitrogen, oxygen, and air to driving pulses with wavelengths from 0.8 to 4 μm, durations from 10 to 500 fs, and intensities from 0.2 to 20 TW/cm^2. In the aim of facilitation of numerical simulations of ultrashort laser-pulse propagation in the atmosphere, we parametrized the molecular response with a damped harmonic oscillator response function and extracted parameter values relevant for the filamentation regime and associated laser-matter interaction. We found the two frequencies characterizing the molecular response of air almost independent of laser wavelength above 1 μm. However, for laser pulses with durations above 75 fs, the molecular Kerr response prevails over the electronic Kerr response for all wavelengths from the near- to the mid-infrared region. Using our parametrized molecular response and a state-of-the-art propagation model, we have shown from numerical simulations of ultrashort laser-pulse filamentation that the pulse dynamics of a mid-infrared laser pulse undergoing filamentation is significantly affected by the molecular response of air. A significant redshift of the harmonics generated during propagation in air is induced by the Raman-Kerr effect.

[1] A. Couairon and A. Mysyrowicz, Phys. Rep. **441**, 47 (2007).

[2] J. Kasparian, M. Rodriguez, G. Méjean, J. Yu, E. Salmon, H. Wille, R. Bourayou, S. Frey, Y.-B. André, A. Mysyrowicz *et al.*, Science **301**, 61 (2003).

[3] I. Dicaire, V. Jukna, C. Praz, C. Milián, L. Summerer, and A. Couairon, Laser Photon. Rev. **10**, 481 (2016).

[4] N. Jhajj, E. W. Rosenthal, R. Birnbaum, J. K. Wahlstrand, and H. M. Milchberg, Phys. Rev. X **4**, 011027 (2014).

[5] J.-C. Diels, R. Bernstein, K. E. Stahlkopf, and X. M. Zhao, Sci. Am. **277**, 50 (1997).

[6] H. Pires, M. Baudisch, D. Sanchez, M. Hemmer, and J. Biegert, Prog. Quantum Electron. **43**, 1 (2015).

[7] G. Andriukaitis, T. Balčiūnas, S. Ališauskas, A. Pugžlys, A. Baltuška, T. Popmintchev, M.-C. Chen, M. M. Murnane, and H. C. Kapteyn, Opt. Lett. **36**, 2755 (2011).

[8] P. Agostini and L. F. DiMauro, Contemp. Phys. **49**, 179 (2008).

[9] P. Panagiotopoulos, P. Whalen, M. Kolesik, and J. V. Moloney, Nat. Photon. **9**, 543 (2015).

[10] A. V. Mitrofanov, A. A. Voronin, D. A. Sidorov-Biryukov, S. I. Mitryukovsky, M. V. Rozhko, A. Pugžlys, A. B. Fedotov, V. Y. Panchenko, A. Baltuška, and A. M. Zheltikov, Opt. Lett. **41**, 3479 (2016).

[11] J. K. Wahlstrand, S. Zahedpour, A. Bahl, M. Kolesik, and H. M. Milchberg, Phys. Rev. Lett. **120**, 183901 (2018).

[12] F. M. Mitschke and L. F. Mollenauer, Opt. Lett. **11**, 659 (1986).

[13] E. T. J. Nibbering, G. Grillon, M. A. Franco, B. S. Prade, and A. Mysyrowicz, J. Opt. Soc. Am. B **14**, 650 (1997).

[14] J. Ortigoso, M. Rodrıguez, M. Gupta, and B. Friedrich, J. Chem. Phys. **110**, 3870 (1999).

[15] M. Kolesik and J. V. Moloney, Phys. Rev. E **70**, 036604 (2004).

[16] A. Couairon, E. Brambilla, T. Corti, D. Majus, O. de J. Ramírez-Góngora, and M. Kolesik, Eur. Phys. J.: Spec. Top. **199**, 5 (2011).

[17] H. Stapelfeldt and T. Seideman, Rev. Mod. Phys. **75**, 543 (2003).

[18] S. Brodersen, High-Resolution Rotation-Vibrational Raman Spectroscopy in *Raman Spectroscopy of Gases and Liquids*, edited by A. Weber Vol. 11 (Springer, Berlin, Heidelberg, 1979), pp. 7–69.

[19] S. Varma, Y.-H. Chen, and H. M. Milchberg, Phys. Rev. Lett. **101**, 205001 (2008).

[20] F. Calegari, C. Vozzi, S. Gasilov, E. Benedetti, G. Sansone, M. Nisoli, S. DeSilvestri, and S. Stagira, Phys. Rev. Lett. **100**, 123006 (2008).

[21] J. Wu, H. Cai, A. Couairon, and H. Zeng, Phys. Rev. A **79**, 063812 (2009).

[22] J. Wu, H. Cai, A. Couairon, and H. Zeng, Phys. Rev. A **80**, 013828 (2009).

[23] J. M. Brown, A. Couairon, and M. B. Gaarde, Phys. Rev. A **97**, 063421 (2018).

[24] J.-F. Ripoche, G. Grillon, B. Prade, M. Franco, E. T. J. Nibbering, R. Lange, and A. Mysyrowicz, Opt. Commun. **135**, 310 (1997).

[25] M. Mlejnek, E. M. Wright, and J. V. Moloney, Opt. Lett. **23**, 382 (1998).

[26] A. Couairon, Eur. Phys. J. D **27**, 159 (2003).

[27] J. H. Marburger, Prog. Quantum Electron. **4**, 35 (1975).